Imaging large arrays of supported lipid bilayers with a macroscope

Edward T. Castellana and Paul S. Cremer[a)]
Department of Chemistry, Texas A&M University, College Station, Texas 77843

(Received 29 January 2007; accepted 19 March 2007; published 8 May 2007)

Herein, the authors present fluorescence resonance energy transfer (FRET) and two-dimensional protein saturation data acquired from spatially addressed arrays of solid supported lipid bilayers (SLBs). The SLB arrays were imaged with an epifluorescence/total internal reflection macroscope. The macroscope allowed 1× imaging and had a relatively high numerical aperture (0.4). Such powerful light gathering and large field of view capabilities make it possible to simultaneously image dozens of addressed SLBs. Three experiments have been performed. First, a 9×7 array of supported lipid bilayer was fabricated and imaged in which each bilayer element was individually addressed. Second, a FRET assay was developed between Texas Red-DHPE (1,2-dihexadecanoyl-*sn*-glycero-3-phosphoethanolamine) and NBD–PE (1,2-dipalmitoyl-*sn*-glycero-3-phosphoethanolamine-*n*-(7-nitro-2-1,3-benzoxadiazol-4-yl)). The concentration of dye could be varied at each address and the value of the Förster radius (7.3 ± 0.6 nm) was easily abstracted. Third, a ligand/receptor recognition assay was designed to show the two-dimensional number density of proteins which can be bound at saturation. It was found for the streptavidin/biotin pair that the protein saturated at the interface above 3 mol % biotin concentration. This corresponded to a two-dimensional footprint of 40 nm^2 for the streptavidin molecule. These results clearly open the door to using individually addressed bilayers for obtaining large amounts of biophysical data at the supported bilayer/aqueous interface. Such abilities will be crucial to obtaining sufficient data for determining the interfacial mechanisms for a variety of membrane/protein interactions. © *2007 American Vacuum Society.* [DOI: 10.1116/1.2732312]

I. INTRODUCTION

Fluorescence microscopy has proven to be an invaluable tool for the investigation of supported lipid bilayers inside microfluidic devices[1–5] and on array-based platforms.[6–14] When combined with total internal reflection (TIR) illumination, this technique becomes even more powerful, allowing for the investigation of surface specific binding events that occur between membrane bound ligands and aqueous proteins containing complementary receptor sites.[4,15,16] Imaging arrays of bilayers with standard fluorescence microscopy has been performed by shrinking the membrane patches to the micron size scale. This technique has been especially valuable for making one-shot equilibrium dissociation constant measurements in which the contents of a linear bilayer array are identical, but the aqueous solutions above them contain various protein concentrations.[10]

While fluorescence microscopy has the advantage of one-shot imaging, it is limited in its field of view. In order to employ a platform with more individually addressable membrane patches, one needs to either shrink the size of the patch or expand the field of view. Excellent methods are now available for creating micron-scale patterns of lipid bilayers.[1,7–10,13,14,17–20] So long as each bilayer in the array is chemically equivalent to the others, patterning can be scaled down to the 1 μm level or even below. On the other hand, there are a limited number of methods available for making arrays with variable contents at each address. One method is to employ laminar flow of vesicle solutions side by side inside a microfluidic device.[1] This creates a gradient of bilayer chemistries that can be confined by a patterned surface. This method is, however, limited in the number of unique chemical constituents that can be patterned. Moreover, spatial control over the patterned membrane array is somewhat difficult. Another method for patterning unique lipid membrane chemistries relies on the use of polydimethylsiloxane (PDMS) stamping and backfilling.[13] Again, this method can fabricate arrays with a few unique chemistries, but spatial alignment limits this number for practical rapid prototyping purposes. Several light directed methods have also been developed for the patterning of lipid bilayers.[7,18,19] Such techniques, however, have not yet been proven for patterning more than a few components.

Fully controlled spatial addressing of lipid bilayers with unique chemistries at each individual location has been achieved by transferring picoliter- and nanoliter-sized droplets of vesicle solutions to a hydrophilic interface patterned within hydrophobic barriers (i.e., the microcapillary injection method).[8] The array size, however, has been typically limited to 3×3 or 4×4 because of the need to pattern all the contents within the field of view that is compatible with imaging by fluorescence microscopy. Very small boxes (<50 μm) become impractical because of the difficulties that arise from pinpoint liquid delivery. In fact, microcapillary injection already becomes tedious to employ for large arrays with individual elements of 250 μm on each side. On the other hand, larger arrays could be achieved more practically if the element size were bigger (i.e., 1×1 mm^2). Such a strategy

a)Author to whom correspondence should be addressed; electronic mail: cremer@mail.chem.tamu.edu

would require the design and construction of an epifluorescence/total internal reflection macroscope.

Standard epifluorescence microscopes often come equipped with low magnification objectives, which certainly allow for large fields of view. The problem associated with conventional microscopes, however, is that the numerical aperture (NA), or light gathering capability, rapidly decreases with decreasing magnification. In order for the magnification to be decreased, the working distance (distance between the objective and the sample) must be increased. By increasing the working distance and maintaining a fixed objective diameter, one unfortunately also reduces the solid angle at which light can be collected from a given point on the sample. Low NA/large field of view imaging therefore requires longer exposure times, which decreases the signal-to-noise ratio and increases the amount of photobleaching in the sample. The solution to this problem is to build a system with large diameter objectives.

Epifluorescence macroscopes employing 1× magnification have been previously developed for imaging animal tissues.[21–23] The basic design uses a tandem-lens imaging system much like those used in x-ray video radiography and up-close photography.[24] Surprisingly, however, such instruments have seen limited employment for imaging protein arrays on chip.[25,26] To the best of our knowledge, a total internal reflection fluorescence macroscope has not previously been developed. Herein, we demonstrate the ability to fabricate dozens of uniquely addressed phospholipid bilayers and image them simultaneously with an epifluorescence (EF)/TIR fluorescence macroscope. This technology is then used to demonstrate fluorescence quenching as a function of probe density as well as a ligand-receptor binding assay. These experiments clearly demonstrate for the first time the ability to array large numbers of bilayers with unique chemistries at each address and employ them in model membrane studies. This should greatly aid biophysical measurements of lipid membrane/protein interactions.

II. METHODS

A. Macroscope design

We have designed a unique low magnification, high NA fluorescence imaging system for monitoring supported phospholipid bilayers. The system is equipped with multiple filter sets that can be rapidly interchanged just like in standard fluorescence microscopy. The macroscope also has a separate port for total internal reflection fluorescence imaging experiments. Additionally, this is the first design of a fluorescence macroscope with exchangeable filter sets. This is made possible by seating the filters and dichroic mirrors on mounts which ride on a system of linear bearings. The movement of the mounts is easily controlled by a rack and pinion drive. In the current setup, we have the ability to image standard red (excitation: 580±20 nm/dichroic mirror: 595 nm/emission: 630±60 nm) and green (excitation: 480±30 nm/dichroic mirror: 505 nm/emission: 535±40 nm) dyes such as Texas Red, NBD, Alexa-594, and Alexa-488. Moreover, the existing filters can be mixed and matched within seconds on the rack and pinion drive to provide fluorescence resonance energy transfer (FRET) imaging. The filter sets used in this setup were larger versions of the standard sets produced by Chroma Technologies (Rockingham, VT) for use in epifluorescence microscopes. Our red and green sets correspond to Chroma set Nos. 41027 and 31001, respectively.

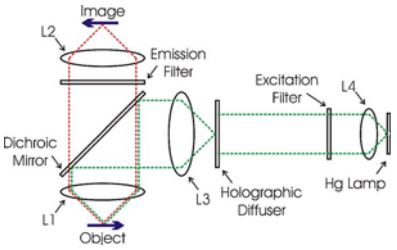

FIG. 1. Epifluorescence imaging pathway in the macroscope. The collimated light from a mercury arc lamp is passed through the excitation filter and illuminates a holographic diffuser. The illuminated holographic diffuser acts as a source for lens L3, which passes a collimated beam to the dichroic mirror. It is then reflected through lens L1 and an image of the diffuser is formed in the plane of the sample. Fluorescence emitted from the sample is colleted by the objective lens (L1) passing through the dichroic mirror and emission filter, and is imaged onto a CCD chip by the imaging lens (L2).

Expanding from the design of Ratzlaff and Grinvald,[21] tandem-lens imaging is performed in our experiments between two lenses where the object is placed at the focal length of the first lens and the image is formed at the focal length of the second lens.[24] Figure 1 shows a schematic illustration of this imaging tandem-lens strategy for epi-illumination. To afford epi-illumination, the light from a 100 W high-pressure mercury arc lamp was collimated by a lens (L4, $f=17$ mm aspheric lens) and passed through an excitation filter onto a holographic diffuser (Edmund Optics, Barrington, NJ). The illuminated holographic diffuser was then imaged onto the plane of the sample via a tandem-lens pair L3 and L1 (85 mm $f/1.4$ Nikon 35 mm SRL lens and 50 mm $f/1.2$ Nikon 35 mm SRL lens, respectively) with the desired illumination wavelengths reflecting off the dichroic mirror in between them. The emitted fluorescence light from the sample was collected by an objective lens, L1, passed through a dichroic mirror and emission filter, and imaged onto a charge coupled device (CCD) camera by the imaging lens (L2, 50 mm $f/1.2$ Nikon 35 mm SRL lens). The CCD camera was a Photometrics SenSys equipped with MetaMorph software from Universal Imaging Corp.

The total internal reflection pathway is shown in Fig. 2. The process of total internal reflection occurs when light propagating through a medium of high refractive index encounters an interface to a second medium of lower refractive index at an angle greater than the critical angle. At the interface, where TIR occurs, an evanescence wave is generated in the second medium and decays exponentially. For lipid bilayers on glass supports under an aqueous solution, the electromagnetic wave penetrates the glass/buffer interface to approximately a depth of 100 nm, exciting only the fluorophores near the solid/liquid interface.[15] TIR illumination is carried out by sliding a smaller dichroic mirror and

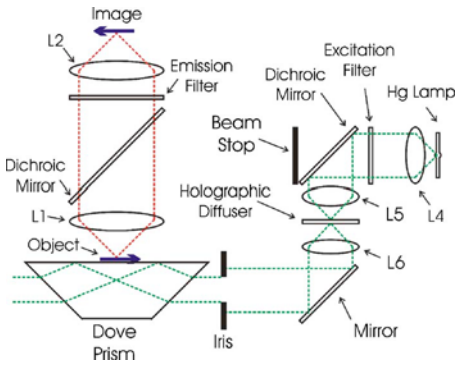

FIG. 2. TIR illumination pathway in the macroscope. The collimated light from a mercury arc lamp is passed through the excitation filter and reflected off a dichroic mirror through lens L5. Lens L5 forms an image of the arc on the holographic diffuser. The illuminated holographic diffuser acts as the source for lens L6, which passes a collimated beam to the aluminum mirror where it is reflected through an iris and into a dove prism. Total internal reflection of the excitation beam occurs at the sample buffer interface, generating an evanescence wave into the sample. Fluorescence emitted from the sample is colleted by the objective lens (L1) passing through the dichroic mirror and emission filter, and is imaged onto a CCD chip by the imaging lens (L2).

beam stop into the epi-illumination beam path immediately after the excitation filter. This diverts the excitation beam down and out of the macroscope where it is focused onto a holographic diffuser by lens L5 (50 mm $f/1.4$ Nikon 35 mm SRL lens). The diffuser is placed approximately at the focal length of lens L6 ($f=30$ mm), to produce a collimated illumination beam. This beam is reflected off an aluminum mirror and passed through an iris before entering a dove prism, where total internal reflection of the beam occurs, allowing for evanescence wave illumination of the sample.

Magnification in a tandem-lens system is calculated by the ratio of the focal length of the imaging lens to the objective lens (L2/L1). Since our system uses two 50 mm $f/1.2$ lenses in tandem, it provides $1\times$ magnification and a numerical aperture of approximately 0.4. Data collected from arrays of supported lipid bilayers (SLBs) are corrected for vignetting by dividing the entire image by an image of a single SLB with an area greater than the field of view of the macroscope (9×7 mm^2). Data are then collected from the corrected image by averaging the intensity at each address. A computer aided design rendering of the inside of the EF/TIR macroscope is shown in Fig. 3.

B. Solid supported lipid bilayers

SLBs are produced by the spontaneous fusion of small unilamellar vesicles (SUVs) to a hydrophilic glass substrate.[27] SUV solutions were made using the following materials: purified water obtained from a NANOpure Ultrapure Water System [Barnstead, Dubuque, IA (18 MΩ/cm^2)]; sodium phosphate and NaCl (Aldrich Chemical Company, Milwaukee, WI); egg phosphatidylcholine (egg PC), NBD-PE, and 1,2-dioleoyl-*sn*-glycero-3-phosphoethanolamine-*N*-(cap biotinyl) (biotin-PE) (Avanti Polar Lipids, Alabaster, AL); and Texas Red-DHPE (Molecular Probes, Inc., Eugene, OR). The production of SUVs was carried out by extruding multilamellar vesicles through polycarbonate filters at high pressures.[28] To do this, lipid mixtures of the desired molar ratios were first mixed in chloroform, dried under a stream of nitrogen, desiccated under vacuum for 2 h, and reconstituted in 10 ml of *p*H 7.2 phosphate buffered saline (PBS) (10 mM sodium phosphate and 140 mM NaCl). Lipid solutions were subjected to ten freezes/thaw cycles in liquid nitrogen to produce multilamellar vesicle dispersions. The multilamellar vesicles were then extruded five times through a 50 nm polycarbonate filter. The average diameter of the SUVs was measured to be 82 nm by dynamic light scattering (90 Plus, Brookhaven Instruments Corp., Holtsville, NY).

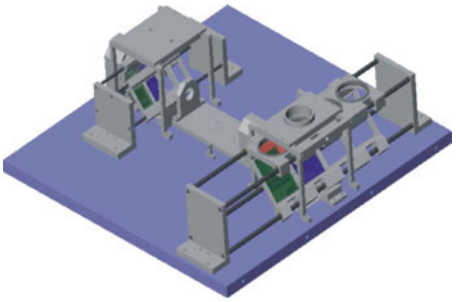

FIG. 3. Internal rendering of the EF/TIR macroscope. The filter and mirror mounts are free to move on a set of linear bearings. Filter sets are easily selected by turning a knob on the outside which moves the rack and pinion drive.

C. Array chip fabrication

Array fabrication was carried out using standard photolithographic techniques. Microscope cover slips, 1 in.^{2}, were boiled in a 10% 7× detergent solution (ICN, Costa Mesa, CA), annealed in a kiln at 450 °C for 5 h and coated with 1000 Å of chrome by metal evaporation (BOC Edwards Auto 306 Metal Evaporation Chamber, Wilmington, MA). An approximately 6 μm thick photoresist coating was spun onto the chrome coated slides and baked at 90 °C for 45 min. A photomask with a square grid array pattern was made with CORELDRAW 9 and reduced onto 35 mm film as negative.[16] UV illumination through the photomask allowed the development of the photoresist, which created a 10×10 array of 0.6×0.6 mm^2 boxes separated by 0.4 mm hydrophobic photoresist walls. The exposed chrome was then removed using a commercial chrome etchant, yielding an array of hydrophilic glass plates with hydrophobic photoresist walls. Microcapillary tips (1.5 mm outside diameter, World Precision Instruments, Sarasota, FL) were used to deliver vesicle solutions to each unique address in the array. In order to achieve this, capillary tubes were pulled in a micropipette puller (Sutter P-97, Sutter Instruments, Novato, CA) to an outer diameter of less than 10 μm. These tips were treated with 1,1,1,3,3,3-hexamethyldisilazane vapor (HMDS) (Aldrich Chemical Company, Milwaukee, WI) in a 75 °C oven to make the surface hydrophobic. This allowed for easy transfer of vesicle solutions from the tip to the glass surface. By attaching the pulled capillary to a 100 μl micropipette, the

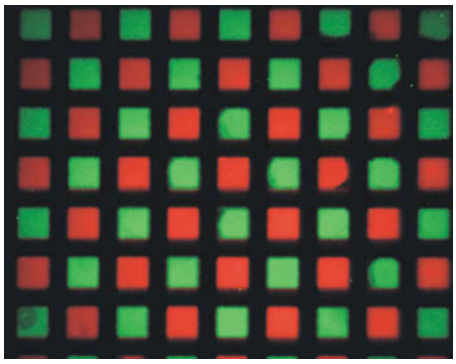

FIG. 4. False color image of an array of phospholipid bilayers addressed with red and green dye labeled SLBs. Each box was 0.6×0.6 mm^2 separated by 0.4 mm hydrophobic walls.

dispensing of droplets to the surface of the array chip could easily be controlled.

III. RESULTS

In a first set of experiments, we wished to demonstrate that it would be possible to easily scale up the microcapillary injection method for creating addressed arrays of phospholipid membranes from previously employed 3×3 and 4×4 formats.[8] For this purpose we chose to address a 10×10 array of boxes with a center-to-center spacing of 1 mm. Figure 4 shows a false color fluorescence image of the array. 63 of the 100 boxes are completely in the frame. This limitation in field of view is caused by the size of the CCD chip (9×7 mm^2).

To perform the addressing, an array chip was placed on a cold plate and the temperature of the chip was adjusted to just above the dew point in order to prevent evaporation of the addressed solutions. A 35 μl SUV sample was drawn into the HMDS coated tip using the micropipette. The tip was then gently touched to the desired array location to expel the aqueous solution via a capillary action. The tip was then cleaned with a water/ethanol solution before the next SUV sample was introduced. Once the array chip was fully addressed, the sample was submerged in purified water to remove excess vesicles. The boxes were addressed with the following solutions: 1 mol % Texas Red-DHPE in egg PC and 5 mol % NBD-PE in egg PC to make the alternating two color pattern shown in Fig. 4. It should be emphasized that addressing this array of 100 boxes (including each individual washing step) took only 20 min because of the large box size. This is a significant advantage when compared to the 1 h needed to address a 4×4 array of smaller boxes.[8,29] Only two unique chemistries were alternated in this particular example; however, it is nearly as easy to employ many unique lipid compositions, as is demonstrated below.

A. Fluorescent resonance energy transfer imaging

The FRET process occurs when an acceptor fluorophore is brought within close proximity of a donor fluorophore.[30] If there is sufficient overlap in the emission spectrum of the donor and the absorbance spectrum of the acceptor, then energy transfer may occur. This process can accurately measure distances for interactions in the 1–10 nm range. Such distances are important, for example, in cellular signaling processes, cell-cell adhesion, and transmembrane protein-protein interactions.[31,32] As a demonstration of this process in our EF/TIR macroscope, we monitored the FRET interactions between NBD-PE and Texas Red-DHPE in SLBs.

Total internal reflection FRET with the EF/TIR macroscope was carried out by combining the green dye excitation filter and dichroic mirror with the red dye emission filter and a dichroic mirror. This is simply done by rack and pinion stirring. A 6×6 section of the array chip was addressed with 36 unique SLB chemistries and then imaged. Along the x axis, the mole fraction of Texas Red-DHPE in the SLBs was varied from 0 to 1.0 mol %, while the mole fraction of NBD-PE was varied from 0 to 5.0 mol % along the y axis. Fluorescent images of the chip in the red, green, and FRET channels are shown in Figs. 5(A), 5(B), and 5(C), respectively. Three-dimensional plots of the normalized fluorescence intensity versus the mol % of each dye present in the membranes are shown in Figs. 5(D)–5(F). As the mole fraction of Texas Red-DHPE was increased, the fluorescence intensity observed in the red channel increased linearly with concentration [Fig. 5(D)]. As expected, this intensity was unaffected by the presence of the NBD-PE. On the other hand, as the mole fraction of Texas Red-DHPE increased, the fluorescence intensity from the NBD-PE observed in the green channel decreased at constant NBD-PE concentration due to the FRET process upon blue excitation [Fig. 5(E)]. Moreover, an increase in the fluorescence emitted from the Texas Red-DHPE was observed in the FRET channel with increasing concentration of NBD-PE [Fig. 5(F)]. In our concentration range, the maximum FRET occurred at the maximum dye concentrations (5 mol % NBD-PE, 1 mol % Texas Red-DHPE). Using data acquired in the FRET image, it was possible to calculate the energy transfer efficiency (E) of the FRET process [Eq. (1)] occurring in an individual element of the array. This was done by using the intensity, F_{DA}, of a given element and dividing it by the maximum intensity possible, $F_{\mathrm{DA\text{-}MAX}}$, which is the intensity at 100% efficiency:[33]

$$E = \frac{F_{\mathrm{DA}}}{F_{\mathrm{DA\text{-}MAX}}}. \tag{1}$$

To obtain $F_{\mathrm{DA\text{-}MAX}}$, the fluorescence in the 5 mol % NBD-PE row was plotted as a function of the number density of Texas Red-DHPE molecules and extrapolated to infinite Texas Red concentration [Fig. 6(A)]. To estimate the spacing R between the NBD-PE/Texas Red-DHPE pair at a given concentration, we assumed that all lipids were 0.60 nm^2 and that the FRET process occurred between a given NBD-PE molecule and only the closest Texas Red molecules in the same leaflet of the bilayer. Using these estimated dye spacings and experimentally determined efficiency values, the Förster radius, R_o, for the dye pair in the membrane could be found from[30]

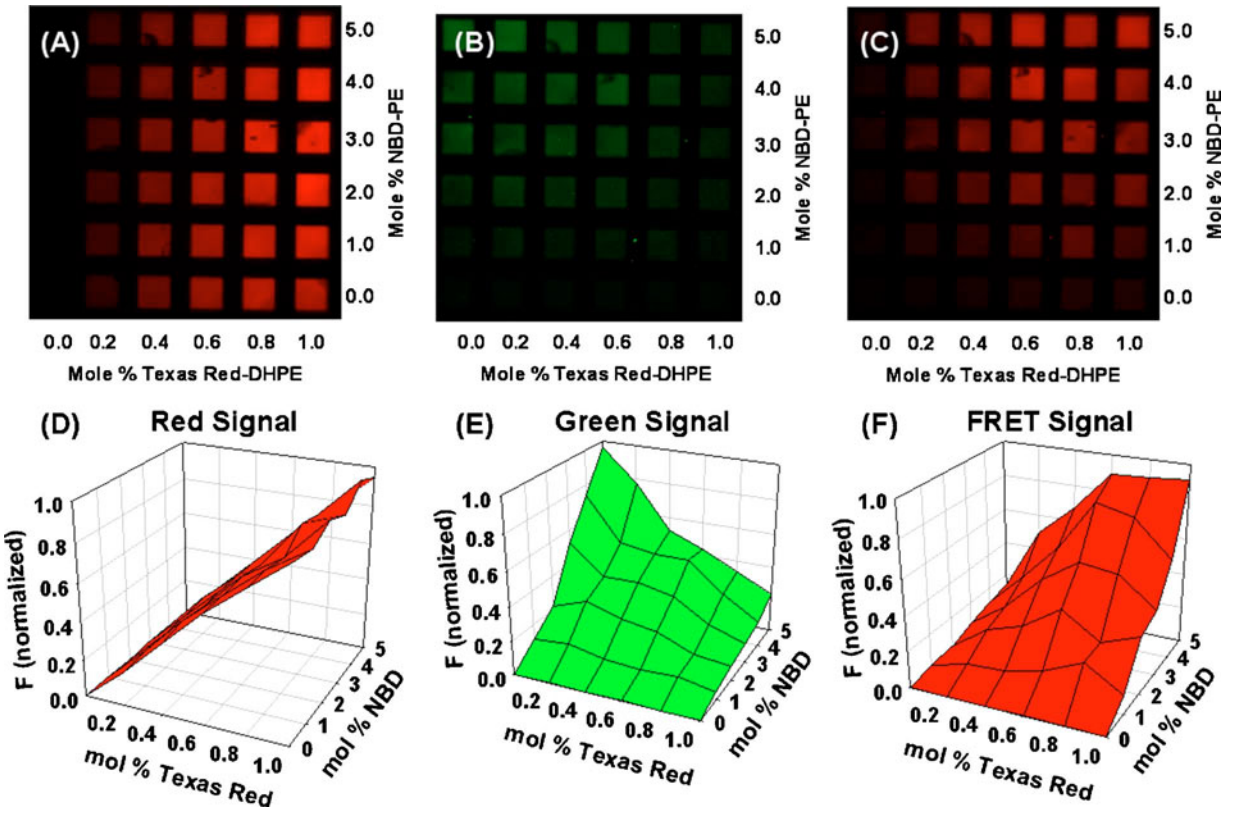

FIG. 5. Images and data from the FRET experiment. Each sample box is 0.6×0.6 mm^2. (A) Red fluorescence image. (B) Green fluorescence image. (C) FRET fluorescence image. (D) Plot of the normalized fluorescence intensity from the red image. (E) Plot of the normalized fluorescence intensity from the green image. (F) Plot of the normalized fluorescence intensity from the FRET image.

$$R = R_o\left(\frac{1}{E} - 1\right)^{1/6}. \tag{2}$$

This was carried out by plotting the estimated dye spacing (R) and the calculated efficiency values (E) as R vs $(1/E-1)^{1/6}$, and fitting the data with equation (2). The value of the slope obtained is R_o [Fig. 6(B)]. The average R_o obtained from the array is 7.3 ± 0.6 nm. This compares quite favorably to the literature value of $R_o = 7.25$ nm.[34] Moreover, this is one of the simplest methods for obtaining such information and demonstrates the power of using SLB arrays. It should be noted that there are more sophisticated means for estimating R and correcting for donor interactions with multiple acceptors;[35,36] however, the use of such methods did not change our results within the experimental error.

B. Ligand density arrays

The saturation coverage of proteins on a lipid membrane surface is a key parameter. At low ligand densities in a lipid bilayer, aqueous proteins may bind to the interface until they saturate all the available binding sites. On the other hand, if enough ligands are present in the membrane, sufficiently large proteins will carpet the entire surface without binding all the ligands presented in the membrane. In this case, the two-dimensional footprint of the incoming protein limits its ultimate coverage. This footprint size can be determined by finding the minimum ligand density at which the aqueous protein carpets the surface. Finding the footprint size also allows fractional coverages to be determined, which can be particularly useful for investigating enzyme kinetics for proteins immobilized at the interface.[37]

As a demonstration of the ability to measure protein footprint sizes in a high throughput fashion, a simple binding experiment was designed. Supported bilayers of egg PC were arrayed on chip with varying ligand densities of biotin-PE ranging from 0 to 5 mol %. The array chip was rinsed with pH 7.2 PBS buffer and then incubated with a 0.1 mg/ml bovine serum albumin solution for 30 min to passivate the surface. Finally, the chip was rinsed with PBS buffer and incubated with a solution containing 4 μM Alexa-488 labeled streptavidin for 3 h. This is well in excess of that needed to achieve binding site saturation.[38] The chip was imaged with the EF/TIR macroscope, and a false color green image is shown in Fig. 7(A). A line scan across a given row (region highlighted with a white dotted box) is shown in Fig. 7(B). As can be seen, the maximum surface coverage for the ligand-receptor pairs occurs near 3 mol % streptavidin. Assuming that (a) the molecular area of a lipid is ~ 0.60 nm^2, (b) the ligands are distributed equally in both the upper and lower leaflets, and (c) the binding of streptavidin is bivalent due to the strong cooperativity,[39] one can estimate the footprint size of streptavidin on the surface. This value is ~ 40 nm^2, which is consistent with literature data from two-dimensionally crystalline streptavidin (33.6 nm^2).[40] As ex-

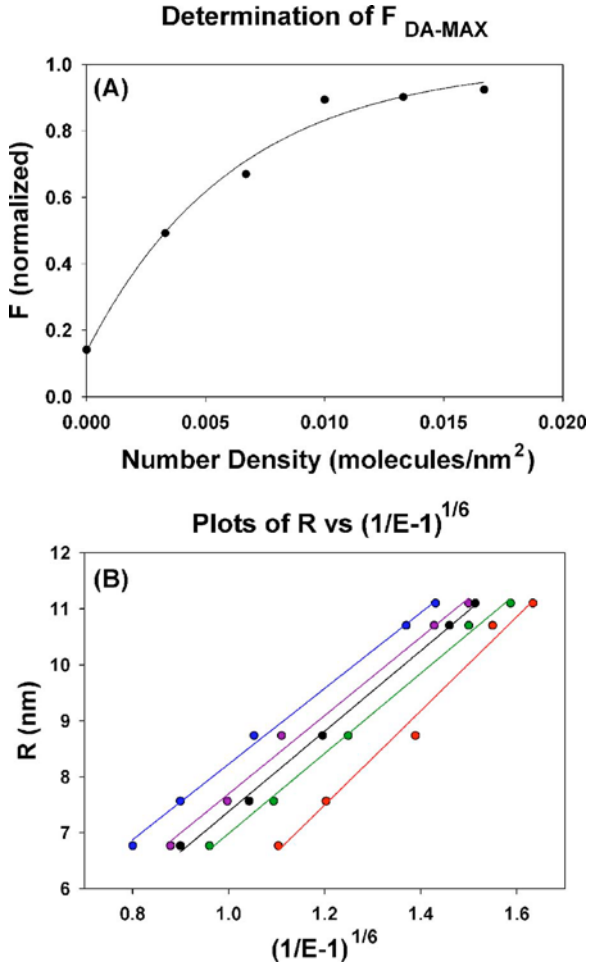

FIG. 6. (A) Determination of $F_{\text{DA-MAX}}$ from the FRET experiment. The normalized fluorescence data were fit with the equation $F([c])=F_o+a(1-e^{-b[c]})$, where $[c]$ is the number density of Texas Red molecules, and a and b are fitting parameters. $F_{\text{DA-MAX}}$ was found by letting $[c]$ approach infinity. (B) Fit of the data from the FRET experiments showing the calculation of the Förster radius (slope).

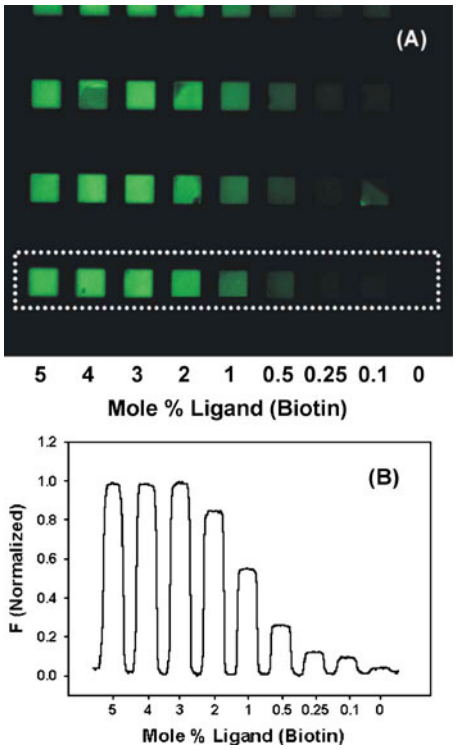

FIG. 7. TIR image of a protein binding assay. Each sample box is 0.6 $\times$ 0.6 mm^2. Decreasing mole fractions of the ligand biotin were addressed from left to right, and all three rows contain identical biotin concentrations. (A) False color image showing the binding of Alexa-488 labeled streptavidin. (B) Line scan across the highlighted boxes in (A).

pected, our value is slightly larger because the streptavidin in the present experiment should not be perfectly packed into two-dimensional crystals.

IV. DISCUSSION

Total internal reflection fluorescence and epifluorescence imaging are important tools for the investigation of lipid membrane interactions with aqueous analytes. For example, utilizing a high density array could allow parameters such as cholesterol content, ligand density, lipid headgroup chemistry, alkyl chain length, and number of sites of unsaturation, as well as net membrane charge to be modulated facilely in a single on-chip format. Epifluorescence could be useful in an array-based format for monitoring two-dimensional protein crystallization of membrane bound proteins as a function of lipid bilayer chemistry. Using streptavidin as a model system, high-throughput array-based analysis may provide further insights into protein-protein interactions at lipid membrane interfaces.[41–45] On the other hand, TIR fluorescence imaging could be employed for monitoring ligand-receptor binding between membrane-bound ligands and aqueous proteins. This would be especially important for multivalent ligand-receptor interactions in fluid lipid bilayers. Such binding events are prevalent in biological processes such as bacterial and viral attacks, human immune response, and signal transduction.[46] One could even monitor the stimulation of *T* cells over a lipid bilayer array with various concentrations of glycosylinositol phospholipid-linked signaling moieties at each address. By varying the concentration of ligands, this assay would enable the rapid determination of the minimum ligand density required for *T*-cell stimulation.[47]

FRET imaging of large membrane arrays will be useful for investigating processes that occur in cellular membranes where changes in distances are important. In particular, this technique could be employed for exploring lipid raft formation,[48] protein-protein interactions,[49] cell-cell interactions,[50] and protein folding.[51] Again, all these processes could be studied in an array-based format by varying a wide variety of membrane constituents.

The number of samples we are currently able to address is limited by the hand addressing techniques being utilized. If the bilayer/macroscope techniques developed herein were combined with existing robotic addressing technologies,[11] the high throughput capabilities of the EF/TIR macroscope could be enhanced even further. More samples per chip would not only allow the rapid collection of larger quantities

of data, but also larger numbers of duplicate samples, increasing the signal-to-noise ratio for biophysical measurements.

ACKNOWLEDGMENTS

The authors thank the National Institutes of Heath (R01-070622) and the Army Research Office (W911NF-05-1-0494) for support.

[1]L. Kam and S. G. Boxer, Langmuir **19**, 1624 (2003).
[2]J. M. Moran-Mirabal *et al.*, Biophys. J. **89**, 296 (2005).
[3]C. R. Poulsen *et al.*, Anal. Chem. **77**, 667 (2005).
[4]T. Yang *et al.*, J. Am. Chem. Soc. **125**, 4779 (2003).
[5]H. B. Mao, T. L. Yang, and P. S. Cremer, J. Am. Chem. Soc. **124**, 4432 (2002).
[6]S. Majd and M. Mayer, Angew. Chem., Int. Ed. **44**, 6697 (2005).
[7]L. A. Kung *et al.*, Adv. Mater. (Weinheim, Ger.) **12**, 731 (2000).
[8]P. S. Cremer and T. L. Yang, J. Am. Chem. Soc. **121**, 8130 (1999).
[9]J. T. Groves, N. Ulman, and S. G. Boxer, Science **275**, 651 (1997).
[10]T. L. Yang, E. E. Simanek, and P. Cremer, Anal. Chem. **72**, 2587 (2000).
[11]V. Yamazaki *et al.*, BMC Biotechnology **5** (2005).
[12]A. R. Sapuri, M. M. Baksh, and J. T. Groves, Langmuir **19**, 1606 (2003).
[13]J. S. Hovis and S. G. Boxer, Langmuir **17**, 3400 (2001).
[14]L. A. Kung *et al.*, Langmuir **16**, 6773 (2000).
[15]L. K. Tamm, in *Optical Microscopy: Emerging Methods and Applications*, edited by B. Herman and J. J. Lemasters (Academic, San Diego, 1993), p. 295.
[16]T. L. Yang *et al.*, Anal. Chem. **73**, 165 (2001).
[17]E. Sackmann, Science **271**, 43 (1996).
[18]C. K. Yee, M. L. Amweg, and A. N. Parikh, J. Am. Chem. Soc. **126**, 13962 (2004).
[19]K. Morigaki *et al.*, Angew. Chem., Int. Ed. **40**, 172 (2001).
[20]B. Ilic and H. G. Craighead, Biomed. Microdevices **2**, 317 (2000).
[21]E. H. Ratzlaff and A. Grinvald, J. Neurosci. Methods **36**, 127 (1991).
[22]S. Sasaki *et al.*, Neuroimage **17**, 1240 (2002).
[23]I. Vanzetta and A. Grinvald, Science **286**, 1555 (1999).
[24]L. Lefkowitz, *The Manual of Close-Up Photography* (American Photographic Book, New York, 1979).
[25]J. C. Yarrow *et al.*, BMC Biotechnology **4** (2004).
[26]M. Bally *et al.*, Surf. Interface Anal. **38**, 1442 (2006).
[27]A. A. Brian and H. M. McConnell, Proc. Natl. Acad. Sci. U.S.A. **81**, 6159 (1984).
[28]M. J. Hope *et al.*, Biochim. Biophys. Acta **812**, 55 (1985).
[29]H. Bayley and P. S. Cremer, Nature (London) **413**, 226 (2001).
[30]L. Stryer, Annu. Rev. Biochem. **47**, 819 (1978).
[31]E. Li and K. Hristova, Langmuir **20**, 9053 (2004).
[32]R. Parthasarathy *et al.*, J. Phys. Chem. B **108**, 649 (2004).
[33]R. M. Clegg, Methods Enzymol. **211**, 353 (1992).
[34]D. E. Wolf *et al.*, Biochemistry **31**, 2865 (1992).
[35]A. K. Kenworthy and M. Edidin, J. Cell Biol. **142**, 69 (1998).
[36]T. G. Dewey and G. G. Hammes, Biophys. J. **32**, 1023 (1980).
[37]H. B. Mao, T. L. Yang, and P. S. Cremer, Anal. Chem. **74**, 379 (2002).
[38]A. Chilkoti and P. S. Stayton, J. Am. Chem. Soc. **117**, 10622 (1995).
[39]X. H. Zhang and V. T. Moy, Biophys. Chem. **104**, 271 (2003).
[40]E. E. Kim and H. W. Wyckoff, J. Mol. Biol. **218**, 449 (1991).
[41]S. A. Darst *et al.*, Biophys. J. **59**, 387 (1991).
[42]F. J. Schmitt *et al.*, Makromol. Chem., Macromol. Symp. **46**, 133 (1991).
[43]A. Schmidt *et al.*, Biophys. J. **63**, 1385 (1992).
[44]S. A. Hemming *et al.*, J. Mol. Biol. **246**, 308 (1995).
[45]L. S. Jung *et al.*, Sens. Actuators B **54**, 137 (1999).
[46]M. Mammen, S. K. Choi, and G. M. Whitesides, Angew. Chem., Int. Ed. **37**, 2755 (1998).
[47]B. Nag *et al.*, Proc. Natl. Acad. Sci. U.S.A. **90**, 1604 (1993).
[48]M. Rao and S. Mayor, Biochim. Biophys. Acta **1746**, 221 (2005).
[49]M. Dziedzicka-Wasylewska *et al.*, Biochemistry **45**, 8751 (2006).
[50]A. P. Wong and J. T. Groves, Proc. Natl. Acad. Sci. U.S.A. **99**, 14147 (2002).
[51]W. F. DeGrado, H. Gratkowski, and J. D. Lear, Protein Sci. **12**, 647 (2003).